nature energy

ARTICLES

PUBLISHED: 4 SEPTEMBER 2017 | VOLUME: 2 | ARTICLE NUMBER: 17143

Sub-ambient non-evaporative fluid cooling with the sky

Eli A. Goldstein, Aaswath P. Raman and Shanhui Fan

Cooling systems consume 15% of electricity generated globally and account for 10% of global greenhouse gas emissions. With demand for cooling expected to grow tenfold by 2050, improving the efficiency of cooling systems is a critical part of the twenty-first-century energy challenge. Building upon recent demonstrations of daytime radiative sky cooling, here we demonstrate fluid cooling panels that harness radiative sky cooling to cool fluids below the air temperature with zero evaporative losses, and use almost no electricity. Over three days of testing, we show that the panels cool water up to 5 °C below the ambient air temperature at water flow rates of 0.2 l min^{-1} m^{-2}, corresponding to an effective heat rejection flux of up to 70 W m^{-2}. We further show through modelling that, when integrated on the condenser side of the cooling system of a two-storey office building in a hot dry climate (Las Vegas, USA), electricity consumption for cooling during the summer could be reduced by 21% (14.3 MWh).

With rapid growth in demand for cooling across the world[1], and the increasing likelihood of extreme heatwaves as a result of climate change in coming decades[2], improving the efficiency of air conditioning and refrigeration systems (hereon referred to as cooling systems) has taken on heightened urgency. From thermodynamics, among other parameters, the efficiency of vapour-compression-based cooling systems is dependent on the temperature of heat rejection to the environment: a lower condenser temperature results in a higher system efficiency. As a rule of thumb, the electricity input into a cooling system is reduced by 3 to 5 % for every 1 °C reduction of the condenser temperature[3]. Often, ambient air is used as the cooling fluid in condensers, in which case the condenser temperature is typically 5 to 15 °C above the ambient dry-bulb temperature[4]. One approach to lower the condenser temperature is to evaporate water into the ambient air[4]. In evaporatively cooled systems, the temperature of heat rejection is determined by the wet-bulb temperature, which is typically much lower than the dry-bulb temperature. However, due to the added complexity (for example, managing water quality and mineral deposition) and higher initial cost of adding evaporatively cooled components (for example, cooling towers), it is often uneconomical for cooling systems smaller than 1 MW_{th} (MW thermal) to be evaporatively cooled[5]. Moreover, the use of evaporative cooling results in significant water loss, 2 l h^{-1} kW^{-1} of cooling (in excess of 17,000 l kW^{-1} of cooling annually), which is a source of concern in water-stressed regions throughout the world. Therefore, it would be very attractive to be able to operate condensers below the dry-bulb air temperature without water loss.

Radiative sky cooling is a mechanism that enables cooling to sub-ambient temperatures without electricity or evaporating water. In this approach, heat is passively rejected to outer space by exploiting the fact that Earth's atmosphere is partially transparent to mid-infrared thermal radiation. Historically, this cooling mechanism was observed only during clear, dry nights and has had limited use in commercial air conditioning and refrigeration systems. Motivated by building-scale efficiency applications, some studies investigated fluid cooling at night using this mechanism, including a few theoretical[6–10] and experimental[11–13] examples. However, demand for cooling is greatest during the day. Achieving sub-ambient radiative cooling during the day, while of great practical interest, proved to be challenging[14] because the radiating surfaces require a combination of high solar reflection and high thermal emission. Recently, photonic surfaces were designed and used to passively reject heat at sub-ambient temperatures during the day, even under direct sunlight[15–18]. The application of radiative cooling to cool a fluid for use in cooling systems, while essential to its broader deployment, has thus far been unexplored.

In this Article, we propose and demonstrate a system that can reduce the condenser temperature below the dry-bulb air temperature with no evaporative water losses. The system builds upon, and significantly extends recent developments in radiative sky cooling. The system enables passive cooling of fluids below the dry-bulb air temperature during the day and at night. When directly coupled to a traditional condenser, the radiative cooling panels can dramatically improve the efficiency of cooling and refrigeration systems. We fabricate and test multiple fluid cooling panels, each with a radiating surface area of 0.37 m^2. We characterize the cooling performance of the panels at multiple flow rates of water, with the water entering the panels at the dry-bulb air temperature. During these experiments, water is passively cooled to 2 °C and 3 °C, respectively, below the dry-bulb air temperature for flow rates of 0.29 l min^{-1} m^{-2} and 0.12 l min^{-1} m^{-2}, during the hottest hours of the day. We also test the panels when connected in series under conditions with peak daytime temperatures greater than 30 °C and over 30% relative humidity. For a total surface area of 0.74 m^2, we observe fluid cooling of 3–5 °C below the dry-bulb temperature for nearly 72 h at a water flow rate 0.2 l min^{-1} m^{-2}. This corresponds to an effective heat rejection rate between 40 and 70 W m^{-2} of radiative cooling surface area. Finally, we also estimate the energy savings when these fluid cooling panels are integrated into a building's cooling system. Over four summer months (May through August of a Typical Meteorological Year) in Las Vegas, Nevada, USA, we show that by covering 60% of the roof on a two-storey commercial office building, 14.3 MWh of electricity could be

Edward L. Ginzton Laboratory, 348 Via Pueblo, Stanford University, Stanford, California 94305, USA. e-mail: aaswath@stanford.edu; shanhui@stanford.edu

© 2017 Macmillan Publishers Limited, part of Springer Nature. All rights reserved.

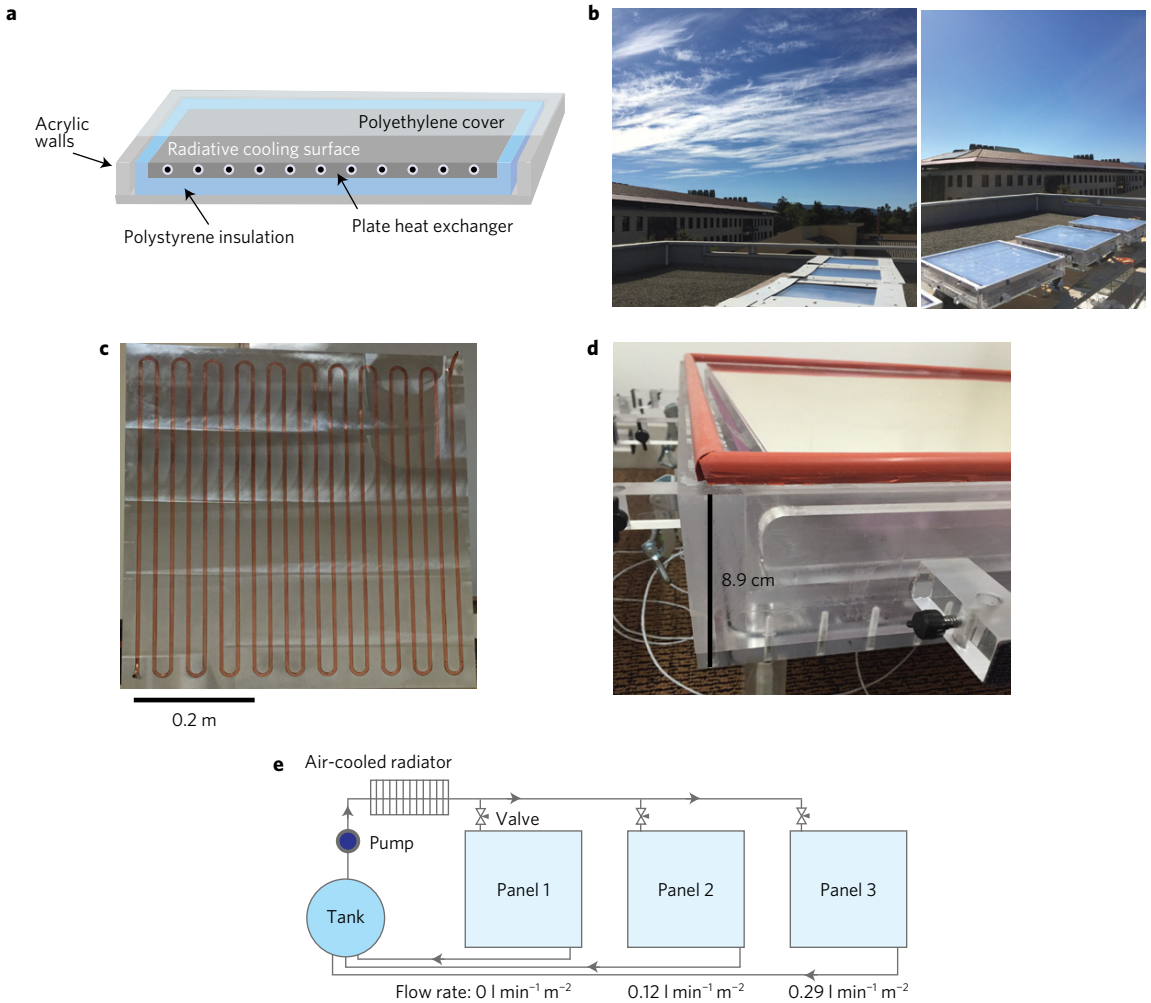

Figure 1 | The fluid cooling panels. a,**b**, Schematic and photographs of the panels and their test configuration on the test rooftop in Stanford, California, USA. **c**, The plate heat exchanger used to transfer heat between the fluid and radiative cooling surface. It consists of a copper tube embedded in an aluminium plate in a serpentine pathway. The aluminium plate heat exchanger has the same surface area as the radiative cooler. **d**, The radiative cooling surface-plate heat exchanger assembly was insulated from the environment by placing it inside a double-walled acrylic enclosure shown here, and a 7.5-μm-thick polyethylene sheet that was stretched over the top of each enclosure as an infrared-transparent wind cover. **e**, A schematic of the piping configuration in the test set-up, highlighting the presence of an air-cooled radiator (to bring the fluid inlet to the panels to the ambient air temperature), pump and tank.

saved, corresponding to a 21% reduction in the electricity required for cooling.

Fluid cooling demonstration

To demonstrate passive, zero-water loss, fluid cooling using the radiative sky cooling mechanism, we fabricated four identical fluid cooling panels. A schematic and photograph of the panels and their test configuration are presented in Fig. 1a,b. Each panel consists of three subsystems: a daytime radiative cooling surface, a plate heat exchanger, and an insulating enclosure. The radiative cooling surface is in thermal contact with the plate heat exchanger and is able to reject heat from the water by having a net radiative heat flux at and below the ambient dry-bulb temperature, even under direct sunlight. To reach sub-ambient temperatures, the cooling surface reflects almost all incident energy from the sun and has strong thermal emissivity in the mid-infrared corresponding to the atmosphere's transparency window (8–13 μm). The plate heat exchanger, which was mated to the radiative cooling surface with thermal paste, is used to establish a thermal pathway between the water in the heat exchanger and the radiative cooling surface. The insulating enclosure is used to thermally isolate the radiative cooling surface–plate heat exchanger assembly from the environment. To capture the full potential of the radiative sky cooling mechanism, the radiative cooling surface is thermally isolated from its local environment, minimizing parasitic ambient heat gain to ensure that the energy being rejected by the panels comes primarily from the water.

In the experiments, the radiative cooling surface employed consists of a visibly-reflective extruded copolymer mirror (3M Vikiuiti ESR film), previously reported to achieve sub-ambient temperatures under sunlight[19], on top of an enhanced silver reflective surface. Each panel has a radiative cooling surface area of 0.37 m^2. The plate heat exchanger, shown in Fig. 1c, consists of a copper tube embedded in an aluminium plate in a serpentine pathway. The plate heat exchanger has the same surface area as the radiative cooling surface. The radiative cooling surface-plate heat exchanger assembly was insulated from the environment by placing it inside a double-walled acrylic enclosure shown in Fig. 1d, and a 7.5-μm-thick polyethylene sheet was stretched over the top of the enclosure as an infrared-transparent wind cover.

During October 2015, we tested three of the fluid cooling panels on a rooftop in Stanford, California, USA. During these tests, the panels were connected in a parallel configuration, whose piping schematic is shown in Fig. 1e. A single pump was used to drive water through all the panels, and valves near the inlet of each panel were

© 2017 Macmillan Publishers Limited, part of Springer Nature. All rights reserved.

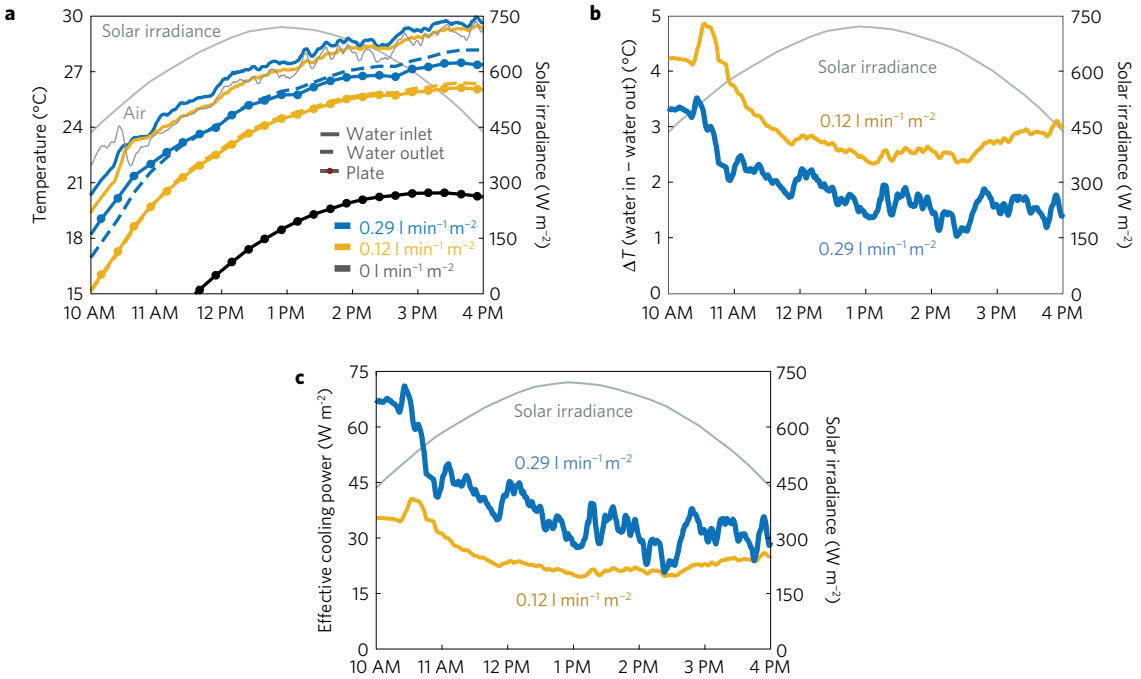

Figure 2 | Water cooling performance versus flow rate. a, Water cooling data for three panels with water flow rates of 0, 0.12 and 0.29 l min^{-1} m^{-2}. The water inlet and outlet temperatures, the plate temperatures of the heat exchanger in each panel, the ambient air temperature and the solar irradiance are plotted. The water inlet temperature tracks the ambient air temperature, while the water outlet and plate temperatures are consistently below air temperature. **b**, A moving average of the difference between the water inlet and outlet temperatures over the same time period is shown for two flow rates, with the slower flow rate panel yielding a temperature reduction of 2.5 °C under greater than 700 W m^{-2} of direct solar irradiance. **c**, The effective fluid cooling power of the panels as determined by the heat capacity of water, the flow rate of water in each panel and the temperature reduction observed (see Methods for details). The faster flow rate yields a higher effective fluid cooling power (nearly 40 W m^{-2} at peak sunlight).

used to control flow rates into each panel. During the experiments, two of the panels had water flowing through them at 0.107 l min^{-1} (0.29 l min^{-1} m^{-2}) and 0.044 l min^{-1} (0.12 l min^{-1} m^{-2}), and the third panel was run with no water to observe the steady-state temperature of the radiative cooling surface. A central tank was used to store water for the experiments. The water, prior to being pumped through the panels, was passed through an air-cooled radiator to cool or heat it, depending on the time of day, to bring the water inlet temperature to the panels close to the ambient dry-bulb temperature.

In Fig. 2, we show the measured water and plate temperatures when the panels were connected in parallel, and exposed to the clear sky between 10 am and 4 pm. The measured air temperature, the water inlet and outlet temperatures, and the plate heat exchanger temperatures of the three enclosures are shown in Fig. 2a, along with the measured solar irradiance. The air-cooled radiator is effectively oversized, allowing us to bring the water inlet temperature of both panels to very near the ambient air temperature. As can been seen in Fig. 2a, the water inlet temperatures track the air temperature well, and allow us to demonstrate the ability of the panels to cool water below the air temperature. The plate temperatures, measured on the underside of the heat exchanger, and the outlet water temperature are well below the air temperature even under greater than 700 W m^{-2} of direct solar irradiance. As expected, the plate temperatures track the outlet water temperature, and display a larger temperature depression relative to ambient for slower flow rates. The panel with no water flowing through it reached the lowest temperature, approximately 7 °C below the ambient air temperature at 12 pm.

The temperature difference between the inlet and outlet water streams for the panels with flowing water is shown in Fig. 2b. For the slower flow rate of 0.12 l min^{-1} m^{-2}, the water temperature decreased nearly 3 °C under peak solar irradiance near 1 pm, while for the faster flow rate of 0.29 l min^{-1} m^{-2} the water temperature decreased by approximately 2 °C. To determine the heat rejection capacity of the panels, we plot in Fig. 2c the effective fluid cooling power delivered to the water, defined as $\dot{m}_{\mathrm{water}} c_{\mathrm{water}} \Delta T$, where $\dot{m}_{\mathrm{water}}$ is the mass of water flowing per second, $c_{\mathrm{water}} = 4.179\ \mathrm{J\,g^{-1}\,K^{-1}}$ is the heat capacity of water and ΔT is the decrease in water temperature through the panel.

The fluid inlet temperature to the higher-flow-rate panel is slightly elevated above the measured air temperature, and shows greater fluctuation relative to the lower-flow-rate panel. The higher-flow-rate panel is further away from the air-cooled radiator, resulting in the inlet temperature being slightly elevated due to ambient heating. However, we note that both the elevation in inlet temperature and difference in fluctuations are near and within, respectively, the accuracy of the temperature probes, which is ±0.3 °C. Thus, while the effect of these fluctuations in inlet temperatures are more clearly seen in Fig. 2b, where we plot the difference between the inlet and outlet temperature, and Fig. 2c, where we use this difference to infer the effective cooling power, the actual fluctuations themselves are less important than the average cooling power during the time period that is observed. Indeed, over the course of the testing period, the slower flow rate panel has an effective fluid cooling power of approximately 20–40 W m^{-2} while the faster flow rate panel, which places a larger heat load on the radiative cooling surface, has an effective fluid cooling power between 30–70 W m^{-2}. This aligns with our expectations that a greater effective fluid cooling power is available at faster flow rates, because the radiative cooling surface has a larger net radiative flux at higher temperatures.

To better illustrate the potential of such fluid cooling systems over a longer period of time, we next present three days of water cooling results from two panels connected in series, when tested in early September 2015 in Stanford, California, USA. As shown in Fig. 3a, the water outlet from the first panel is directly connected

© 2017 Macmillan Publishers Limited, part of Springer Nature. All rights reserved.

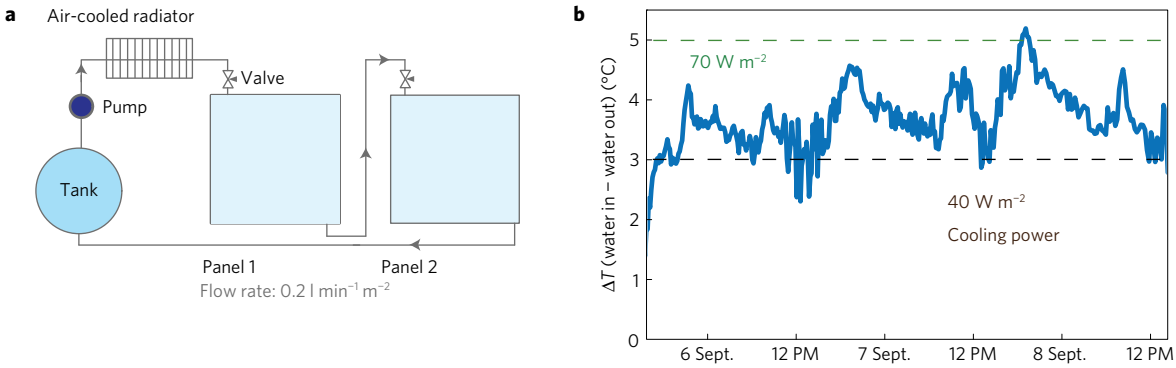

Figure 3 | Extended testing over three days. a, Two of the previously described water cooling panels were connected in series, with the outlet of the first panel directly fed into the inlet of the second panel. An air-cooled radiator sets the water inlet temperature of the first panel to the air temperature. **b**, Three days of data showing the temperature difference between the outlet and inlet of the two panels at a flow rate of 0.2 l min^{-1} m^{-2}. During these three days, peak air temperatures were between 30 °C and 35 °C, with relative humidity during peak daytime hours around 30%. Remarkably 3–5 °C of cooling is consistently seen over these three days. To highlight the effective fluid cooling power, lines are plotted for 40 and 70 W m^{-2}, which roughly delineate the observed performance over these three days.

to the inlet of the second panel, providing a total effective surface area of 0.74 m^2. Over the three days of testing, the solar irradiance exceeded 900 W m^{-2}, the air temperatures peaked above 30 °C and the relative humidity was greater than 30% during the middle of the day. Remarkably, a temperature decrease of the water between 3 °C to 5 °C below the ambient air temperature was observed for a flow rate of 0.2 l min^{-1} m^{-2}, as can be seen in Fig. 3b. This corresponds to an effective fluid cooling power between 40 and 70 W m^{-2} over nearly 72 h of continuous operation.

Modelling panel performance

We developed a transient thermal model to predict the performance of the fluid cooling panels under different weather conditions. The details of the modelling can be found in the Methods section. Using the experimentally measured ambient temperature and solar irradiance data, and an estimate of the non-radiative parasitic heat loss (see Methods), we were able to predict the measured plate temperatures for various flow rates, within 0.5 °C as is shown in Fig. 4. In this figure, the model predictions are given by the dashed lines, and the measured temperatures given by the blue, yellow and black coloured bands.

We next used the panel transient model to predict the performance of fluid cooling panels in the climate of Las Vegas, Nevada, USA. As can be seen in Fig. 5a, employing Typical Meteorological Year (TMY3) data[20] for Las Vegas, we estimate an even greater temperature drop for water flow rates of 0.1 l min^{-1} m^{-2} through 0.3 l min^{-1} m^{-2} for June 1 of the TMY3 dataset, than that observed in our experimental data. The predicted results, and embodied cooling power, are better than the experimental performance in Stanford, California, USA due to: the lower moisture content in the air, which results in greater atmospheric transparency in the mid-infrared window; and higher temperatures, which result in larger blackbody spectral radiances from the radiative cooling surfaces. We can furthermore use this model to understand the various modes of heat transfer present in the panels, and extrapolate longer-term performance, as shown in Fig. 5b,c respectively, for June 1 and 2 from the TMY3 dataset for Las Vegas.

Cooling system energy savings

One important application of these panels is to reject heat as a condenser in a cooling system, thus improving the system's efficiency relative to a standard air-cooled chiller. To that end, we modelled the cooling load for a two-storey reference commercial office building (3,330 m^2 floor area) located in Las Vegas where 60% of the roof is assumed to be covered by the aforementioned

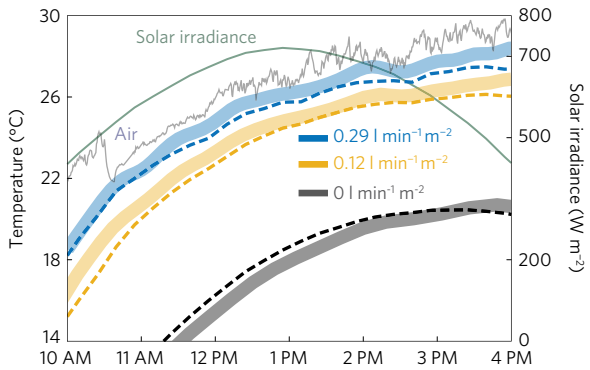

Figure 4 | Modelling performance. Calculations from a non-steady-state thermal model (see Methods) versus observed experimental plate temperatures (from Fig. 2). Using the experimentally measured ambient air temperature, solar irradiance, and an overall heat-transfer coefficient for non-radiative parasitic heat exchange (see Methods), we predict the measured plate temperatures for various flow rates, within 0.5 °C. In this figure, the model predictions are given by the dashed lines, while the measured temperatures given by the blue, yellow and black coloured bands.

fluid cooling panels. Buildings of this size typically use air-cooled chillers (schematically shown in Fig. 6a) which become less efficient as the air temperature rises, which is when grid electricity is in highest demand. In our model, schematically shown in Fig. 6b, the fluid cooling panels are used to generate sub-ambient temperature fluid (water/glycol solution) that is used to remove heat from the condenser of the vapour-compression cooling system used in the two-storey commercial building. The baseline building has a black asphalt roof, and in the calculations we do not account for the reduced cooling load that would come from the roof's albedo having increased due to the presence of the fluid cooling panels, which are highly reflective.

We show in Fig. 6c the building's daily-averaged cooling load and in Fig. 6d the predicted electricity savings resulting from lowering the condenser temperature in the vapour-compression system. For this calculation, fan and pump power in the air-cooled and panel-cooled systems were accounted for in the overall electricity savings. Based on TMY3 data[20] for the summer months (May–August), we calculate that the implementation of the fluid cooling panels would save 14.3 MWh of electricity, a 21% reduction in electricity used for cooling by the building. The energy savings during a day depend on the cooling load required by the building and the

© 2017 Macmillan Publishers Limited, part of Springer Nature. All rights reserved.

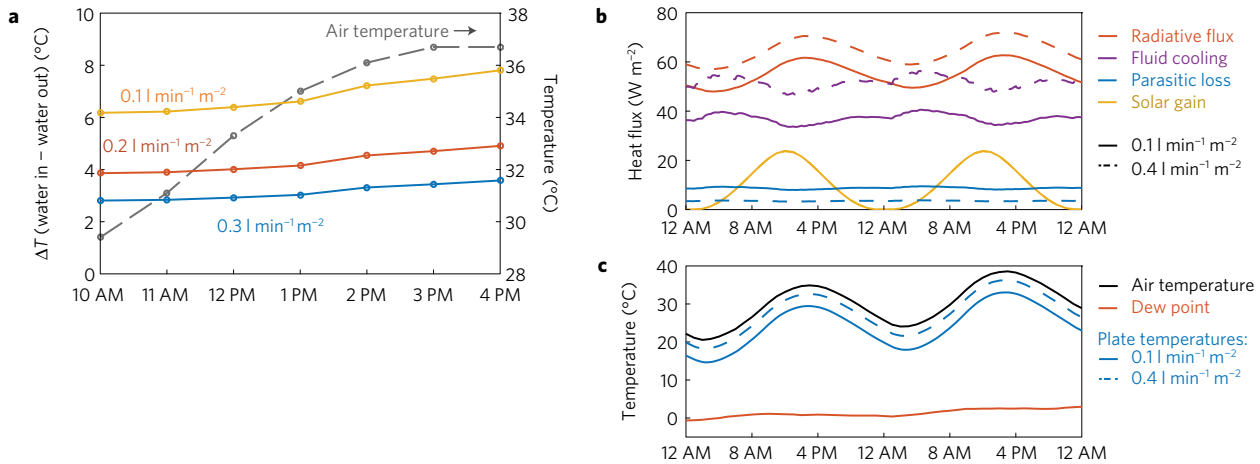

Figure 5 | Fluid cooling performance and heat flows. a, As an example of the fluid cooling panel model's predictive capability we here show its modelling of the temperature reduction possible at three different flow rates with data from June 1 of the Typical Meteorological Year (TMY3) dataset for Las Vegas, Nevada, USA used for environmental conditions. The air temperature is also plotted with its axis on the right. **b**, To elucidate the key energy flows into and out of the panels, we can also use the same model to calculate the various heat fluxes relevant to the fluid cooling panels, here shown for June 1 and 2 of the TMY3 dataset for Las Vegas. The radiative, fluid cooling, solar gain and parasitic loss fluxes per unit area of radiating surface are plotted for two flow rates, 0.1 l min^{-1} m^{-2} (solid) and 0.4 l min^{-1} m^{-2} (dashed), of water flowing through the panels. **c**, The plate temperature for the same flow rates relative to the dry-bulb air temperature and the dew point temperature, illustrating variation relative to air temperature through the course of a day.

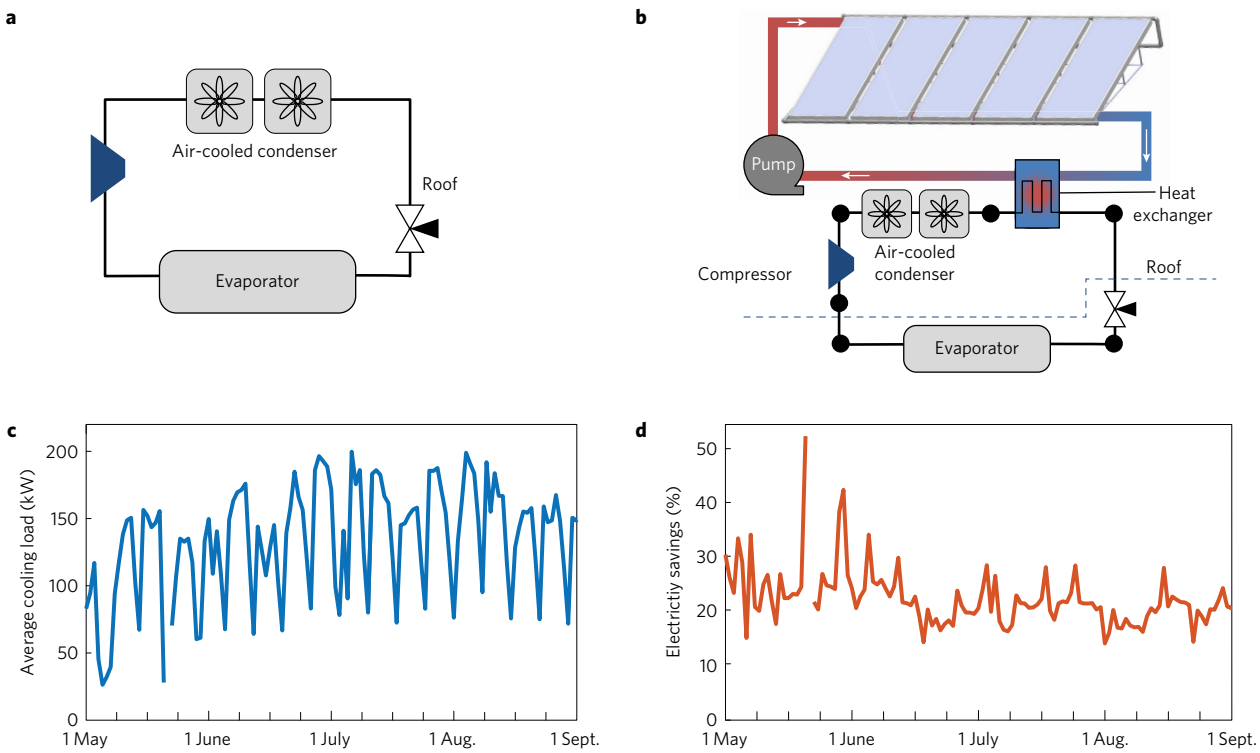

Figure 6 | Modelling cooling system-level energy savings. a,**b**, To assess the capability of the fluid cooling panels to reduce electricity consumption in air-cooled vapour-compression cooling systems, we rigorously model (see Methods) the performance of a conventional baseline air-cooled cooling system (**a**) and a panel-cooled cooling system (**b**), where the panels address part of the condenser load to lower the overall condenser temperature. **c**, The average daily cooling load for a two-storey office building, based on *EnergyPlus* modelling, in Las Vegas, Nevada, USA from May 1 to September 1 of the TMY3 dataset. **d**, The fluid cooling panel model shown in Figs 4 and 5 was used, along with a model of a building's cooling system (see Methods) to predict energy savings relative to an air-cooled chiller, for the building, time frame and dataset used in **c**. The predicted electricity savings from reduced compressor and fan work results in a total of 14.3 MWh in saved electricity over four summer months.

ambient conditions. The daily electricity savings over this period was as low as 18% and as high as 50%. The implementation studied here is a preliminary exploration of how radiative sky cooling can improve cooling system efficiency. While it does hold the potential for impressive energy savings, the scenario considered has not been optimized for cost and payback period. Optimizing the size of the system and mode of integration for payback period, and accounting for balance of system (piping, pumps and heat exchangers), soft and installation costs, will be important for future commercialization and demonstrations.

© 2017 Macmillan Publishers Limited, part of Springer Nature. All rights reserved.

Conclusion

The fluid cooling panels demonstrated here offer a passive, zero-water-loss solution to the vexing challenge of cooling water to sub-ambient temperatures. Beyond water, such approaches can also be used to directly cool other relevant fluids such as glycol or conventional refrigerants to below ambient. Furthermore, with electricity needed only for pumping fluids through the panels, the essentially passive nature of our fluid cooling system is a striking corollary to solar water heating systems. While we have highlighted the system's capability of functioning during the day, thereby addressing cooling system inefficiencies that arise with hot ambient air temperatures, it should be emphasized that the fluid cooling panel functions 24 h a day. Thus, with thoughtful system design and the use of thermal storage at night, when cooling demands may be low or non-existent, even larger energy savings can be extracted from the fluid cooling panels.

A recent study by Fernandez *et al.* suggested that using our panels in combination with indoor radiant cooling systems and thermal storage, could reduce building electricity use for cooling between 45% and 68% relative to today's standard systems in five climate zones[21]. While the mode of integration presented by Fernandez *et al.* yields greater electricity savings (45% in Las Vegas) than the condenser cooling mode described here, we believe using the panels as a condenser is more broadly applicable to building cooling systems than relying on indoor radiant cooling and thermal storage systems; two technologies that have limited deployment due to higher installation costs. If radiative sky cooling is to be widely deployed, it needs to be shown with field tests that the panels can meet relevant financial return paybacks. While competition for roof space is a potential concern, we anticipate that, early on, the cooling panels will complement solar panels by occupying areas of a roof subject to shadowing (for example, north-facing parts of a roof in the Northern Hemisphere).

More generally, coupling radiative cooling systems to other energy systems represents a largely unexplored opportunity for new device and system-level approaches to energy efficiency and generation. From off-grid scenarios, to power plants and industrial facilities, our results show how the radiative coldness of the sky can be integrated with energy systems here on the surface of the Earth to deliver meaningful energy savings.

Methods

Fluid cooling panel fabrication & testing. The plate heat exchanger is fabricated from an aluminium plate of dimensions 610 mm × 610 mm × 7.6 mm (8 kg), with an embedded copper tube of nominal diameter 6.35 mm and total length of 15.5 m. The radiative cooling surface used in these experiments was affixed to the topside of the plate heat exchanger (for example, the side without the copper tubing) with a thermally conductive adhesive. The nominal conductivity of the adhesive is 2 W m^{-1} K^{-1}. A piece of Styrofoam, 25.4 mm thick, was bonded to the backside of the heat exchanger to further insulate the heat exchanger from the air inside the enclosure.

The walls of the enclosure were made of acrylic sheets nominally 6.35 mm thick with an air gap of 12.7 mm between them. The base of the enclosure has thicker walls, 12.7 mm, and an air gap of 18 mm, and the total weight of one acrylic case is 10 kg. To insulate the radiator from wind and water condensation from the ambient air, a top cover made of polyethylene nominally 7.5 μm thick was stretched over the top opening of the enclosure. Additionally, to remove moisture from inside the enclosure during the experiments, desiccant cartridges were placed inside the enclosure underneath the radiative cooling surface. During the experiments, sunshades were also mounted around the periphery of the enclosure; this was done to prevent the sun from heating up the enclosure walls during the day. The shades did not block the radiative cooling surface from the sun and they are not necessary at night. The sky-exposed area after the sunshade is attached is 580 mm × 580 mm. The ultimate form factor of these panels, while satisfactory to demonstrate the technology, require substantial development before becoming a commercial product.

The temperature of the water entering and leaving each enclosure was measured inline with the flow, using 4-wire Class A resistance temperature detectors (RTDs) and the temperatures were recorded with a National Instruments CompactDAQ system. Additional Class A 3- and 4-wire RTDs were also attached at various locations inside the enclosure and attached on the centre of the bottom side of the aluminium plate heat exchanger. To ensure ambient air temperature was accurately measured under rooftop conditions, the RTD used to measure the ambient air temperature was kept shaded from the sun but still exposed to ambient air flow. Additionally, the rooftop area under the panels was covered with a white tarp to further reduce the influence of solar heating. Temperature measurements were made every 30 s and the class A RTDs have an accuracy of 0.3 °C, while the 3-wire RTDs have an accuracy of 0.8 °C. The incident solar flux was recorded during a given experiment with a CMP-6 Pyranometer by Kipp and Zonen, with a directional response of <20 W m^{-2}.

Data sampling was conducted every 30 s, where the data shown in the figures is plotted with a moving average. The final flow rates used in the experiment were measured based on the amount of fluid flowing measured in a graduated cylinder for two minutes at the beginning and end of the experiments. No measurable variation in the flow rate was noted. When calculating the heat rejection from the panels, this flow rate was used to determine the panel's heat rejection rate. The fluid temperatures were measured with an inline temperature probe. A direct measurement of the radiator temperature was not possible. If an RTD were placed on the radiative cooling surface, the RTD would likely heat up under exposure to the sun and would block the radiative cooling surface from emitting energy to the sky. The centre plate heat exchanger temperature thus gives a reasonable estimate of the effective surface temperature for the plate. For the materials and geometries used in the radiative cooling surface-plate heat exchanger assembly, the overall thermal resistance between the cooling surface and the backside of the plate heat exchanger (where the temperature is measured) is of the order 10^{-3} K W^{-1}, indicating a small temperature drop between the surface and the plate. The centre temperature and the fluid outlet temperature were often very similar; however, there is some temperature gradient along the plate as the fluid enters at the ambient air temperature and is cooled along the length of the copper tube.

The inferred cooling power per unit area plotted in Figs 2 and 3 is determined by the following formula:

$$P_{\text{cooling}} = \frac{m_{\text{water}} \times c_{\text{p}} \times \Delta T}{\text{Area}} \tag{1}$$

Here, m_{water} is the mass flow rate of water in units of g s^{-1}, c_{p} is the heat capacity of water and ΔT, the temperature difference between the inlet fluid temperature and the outlet fluid temperature of the panels.

Transient model of fluid cooling systems. To model the fluid panels we consider the dominant heat-transfer pathways to the radiative cooling surface–plate heat exchanger assembly: the emission of thermal radiation from the radiative cooling surface $Q_{\text{radiative cooling}}$; solar heating Q_{solar}; parasitic heating by convection and conduction from the environment $Q_{\text{parasitic}}$; and energy transfer from the flowing water $Q_{\text{fluid cooling}}$. In this model, we assume the plate radiates with an effective temperature and apply the lumped capacitance method to predict its temperature as a function of time.

The set of equations that were solved to predict the fluid and plate temperatures are given by equations (1)–(6) below. The radiative cooling power of surface $Q_{\text{radiative cooling}}$ is a function of the dry-bulb temperature, the dew point, which is a measure of the absolute moisture content in the atmosphere, cloud coverage and cloud height. The solar heat flux Q_{solar} is given by equation (4), where I_{sun} is the incident solar irradiance which is multiplied by the area of the radiator A_{radiator}, τ_{cover} is the transparency of the top cover and α_{radiator} is the absorptivity of the radiative cooling surface. The parasitic heat flux $Q_{\text{parasitic}}$ is given by equation (5), where h_{L} is an overall heat-transfer coefficient that accounts for heat transfer from the environment to the radiative cooling surface by convection and conduction. h_{L} is fitted with the data presented in the experimental section and was found to be nominally 1.5 W m^{-2} K^{-1}. This value of h_{L} was corroborated by developing a one-dimensional thermal resistance model assuming the dimensions of our enclosure. The heat transfer associated with cooling water through the panels is given by equation (6), where $\dot{m}$ is the mass flow rate of water, c_{p} is the heat capacity of water and $T_{\text{water,in}}$, $T_{\text{water,out}}$ the temperature of water in and out of the plate heat exchanger, respectively.

$$m_{\text{plate}} c_{\text{p, plate}} \frac{\text{d}T}{\text{d}t} = Q_{\text{radiative cooling}}(t) - Q_{\text{solar}}(t) - Q_{\text{parasitic}}(t) - Q_{\text{fluid cooling}}(t) \tag{2}$$

$$Q_{\text{radiative cooling}}(t) = f(T_{\text{dry bulb}}, T_{\text{dew point}}) \tag{3}$$

$$Q_{\text{solar}}(t) = \alpha_{\text{radiator}} \tau_{\text{cover}} I_{\text{sun}} A_{\text{radiator}} \tag{4}$$

$$Q_{\text{parasitic}}(t) = h_{\text{L}} A_{\text{radiator}} (T_{\text{dry bulb}} - T_{\text{radiator}}) \tag{5}$$

$$Q_{\text{fluid cooling}}(t) = \dot{m} c_{\text{p, water}} (T_{\text{water in}} - T_{\text{water out}}) \tag{6}$$

© 2017 Macmillan Publishers Limited, part of Springer Nature. All rights reserved.

The differential equation given by equation (2) was integrated as a function of time to predict the plate temperature throughout the day. The dry-bulb air temperature, dew point temperature, solar irradiance, and water inlet temperature were inputs to the model and varied as a function of time during the day. To demonstrate the predictive capabilities of the model, the net radiative heat flux $Q_{\text{radiative cooling}}$, the corresponding fluid cooling $Q_{\text{fluid cooling}}$, solar absorption Q_{solar} and parasitic heat flux $Q_{\text{parasitic}}$ for the two flow rates, over June 1 and June 2 from the Las Vegas TMY3 dataset are shown in Fig. 5b. It can be seen that the higher-flow-rate panel has a higher radiative heat flux and transfers more heat to the fluid ($Q_{\text{fluid cooling}}$) than the low-flow-rate panel. This is predicted because the high-flow panel is warmer and has a higher mass flow rate than the low-flow panel (see equation (6) for $Q_{\text{fluid cooling}}$'s dependence on flow rate). Also illustrated in Fig. 5b is that the lower-flow-rate panel has larger parasitic heat loss. This is because the lower-flow-rate panel has a larger temperature difference from the dry-bulb temperature (for example, it is colder than the high-flow-rate panel). In Fig. 5c we show the corresponding plate temperatures of the radiative cooler for two flow rates (0.1 and 0.4 $\text{l min}^{-1}\,\text{m}^{-2}$) relative to the dry-bulb air temperature and the dew point. As expected and shown in Fig. 5c, the lower-flow rate results in a lower plate temperature relative to the dry-bulb temperature.

Commercial building cooling system modelling. The reference cooling system analysed in these calculations is based on a modified version of the medium commercial building benchmark model defined by the US Department of Energy[22]. While the medium commercial building benchmark has three storeys, the building we modelled has two storeys and a total floor area of 3,330 m^2 (35,800 ft^2). Otherwise, the model is identical to the benchmark model and represents the standard technological approach used to cool a medium-sized commercial building. The hourly cooling load of the building under consideration was estimated using *EnergyPlus*, a whole building energy software package developed by the Building Technologies Office of the US Department of Energy, and is shown in Fig. 6c.

Thermodynamic diagrams of the baseline and modified cooling systems are illustrated in Fig. 6a and 6b, respectively. The panel-cooled fluid loop is comprised of the panels, a pump and a plate heat exchanger. To estimate the energy savings resulting from the addition of the panels, the two cycles were analysed with a model developed in Matlab, and the properties of the refrigerant into and out of each component were determined as a function of time throughout the summer.

The refrigerant used in the system is R134A and the fluid flowing through the panels a 15% ethylene glycol–water solution. The pumps and compressors were modelled with isentropic efficiencies of 70%. The evaporator temperature in both systems was set to 6.67 °C. A 1% pressure drop was assumed for the refrigerant across the condenser, evaporator and plate heat exchanger, and the pressure drop of the ethylene glycol–water solution through the panel array is based on current panel geometry and hydraulic network analysis of the panels connected together in series and parallel. The fan power consumption and flow were modelled based on the fan affinity relations, fan power is proportional to the fluid flow cubed, assuming the fans to be free discharge and variable speed. A total of four fans were used in the system, where each fan has a peak power of 1.9 kW, generating 4,900 l s^{-1} of air flow. The air flow generated by the fans and ethylene glycol–water flow through the panels was determined based on the cooling load required by the building, and for optimum system efficiency.

In the panel modified system (Fig. 6b), a counter flow plate heat exchanger was modelled and is used to transfer heat from the hot refrigerant to the cooler circulating ethylene glycol–water solution flowing through the panels. When the panels are used, they reject the majority of the heat from the condenser, with part of the cooling load (cooling the refrigerant from a superheated vapour to a saturated vapour) rejected by the fans. For the baseline cooling system, a pinch point of 1.7 K was assumed to ensure the refrigerant temperature was never lower than the ambient air temperature. The net energy savings are based on the electricity required to run the compressors, fans and pumps in the two systems.

Data availability. The data that support the plots within this paper and other findings of this study are available from the corresponding authors upon reasonable request.

Received 31 August 2016; accepted 26 July 2017; published 4 September 2017

References

1. Isaac, M. & van Vuuren, D. P. Modeling global residential sector energy demand for heating and air conditioning in the context of climate change. *Energy Policy* **37,** 507–521 (2009).
2. Meehl, G. A. & Tebaldi, C. More intense, more frequent, and longer lasting heat waves in the 21st century. *Science* **305,** 994–997 (2004).
3. Facius, T. *Benefits of Water Cooled vs Air Cooled Equipment in Air Conditioning Applications* Tech. Rep. (Cooling Technology Institute, 2011); http://www.cti.org/downloads/watervsair.pdf
4. *2016 ASHRAE Handbook: Heating, Ventilating, and Air-Conditioning: Systems and Equipment SI Edition* (ASHRAE, 2016).
5. Naguib, R. Total cost of ownership for air cooled and water-cooled chiller systems. *ASHRAE J.* **51,** 42–48 (2009).
6. Sima, J., Sikula, O., Kosutova, K. & Plasek, J. Theoretical evaluation of night sky cooling in the Czech Republic. *Energy Procedia* **48,** 645–653 (2014).
7. Hanif, M., Mahlia, T., Zare, A., Saksahdan, T. & Metselaar, H. Potential energy savings by radiative cooling system for a building in tropical climate. *Renew. Sustain. Energy Rev.* **32,** 642–650 (2014).
8. Qingyuan, Z. & Yu, L. Potentials of passive cooling for passive design of residential buildings in China. *Energy Procedia* **57,** 1726–1732 (2014).
9. Sameti, M. & Kasaeian, A. Numerical simulation of combined solar passive heating and radiative cooling for a building. *Build. Simul.* **8,** 239–253 (2015).
10. Dobson, R. T. Thermal modelling of a night sky radiation cooling system. *J. Energy Southern Afr.* **16,** 20–31 (2005).
11. Meir, M., Rekstad, J. & Løvvik, O. M. A study of a polymer-based radiative cooling system. *Sol. Energy* **73,** 403–417 (2002).
12. Al-Nimr, M., Tahat, M. & Al-Rashdan, M. A night cold storage system enhanced by radiative cooling—a modified Australian cooling system. *Appl. Therm. Eng.* **19,** 1013–1026 (1999).
13. Bourdakis, E., Péan, T. Q., Gennari, L. & Olesen, B. W. Daytime space cooling with phase change material ceiling panels discharged using rooftop photovoltaic/thermal panels and night-time ventilation. *Sci. Technol. Built Environ.* **22,** 902–910 (2016).
14. Nilsson, T. M. & Niklasson, G. A. Radiative cooling during the day: simulations and experiments on pigmented polyethylene cover foils. *Sol. Energy Mater. Sol. Cells* **37,** 93–118 (1995).
15. Rephaeli, E., Raman, A. & Fan, S. Ultrabroadband photonic structures to achieve high-performance daytime radiative cooling. *Nano Lett.* **13,** 1457–1461 (2013).
16. Raman, A. P., Anoma, M. A., Zhu, L., Rephaeli, E. & Fan, S. Passive radiative cooling below ambient air temperature under direct sunlight. *Nature* **515,** 540–544 (2014).
17. Zhai, Y. *et al.* Scalable-manufactured randomized glass-polymer hybrid metamaterial for daytime radiative cooling. *Science* **355,** 1062–1066 (2017).
18. Kou, J.-l., Jurado, Z., Chen, Z., Fan, S. & Minnich, A. J. Daytime radiative cooling using near-black infrared emitters. *ACS Photon.* **4,** 626–630 (2017).
19. Gentle, A. R. & Smith, G. B. A subambient open roof surface under the mid-summer sun. *Adv. Sci.* **2,** 1500119 (2015).
20. Wilcox, S. & Marion, W. *Users Manual for TMY3 Data Sets* (National Renewable Energy Laboratory Golden, 2008).
21. Fernandez, N., Wang, W., Alvine, K. J. & Katipamula, S. *Energy Savings Potential of Radiative Cooling Technologies* Tech. Rep. PNNL24904 (Pacific Northwest National Laboratory, 2015); https://www.osti.gov/scitech/biblio/1234791
22. Deru, M. *et al. US Department of Energy Commercial Reference Building Models of the National Building Stock* Tech. Rep. NREL/TP-5500-46861 (National Renewable Energy Laboratory, 2011).

Acknowledgements

This work is supported by the Advanced Research Projects Agency-Energy (ARPA-E), Department of Energy (Contract No. DE-AR0000316). We are grateful to Z. Weiner, D. Cotugno, R. Shrestha, E. D. de Maricourt and M. Metlitz for their help in fabricating the panels, and assisting with testing.

Author contributions

E.A.G. and A.P.R. are co-first authors and contributed equally. All authors contributed to the conception and design of the experiments. E.A.G. and A.P.R. executed the experiments. All authors wrote the paper. A.P.R. and S.F. are co-corresponding authors.

Additional information

Reprints and permissions information is available at www.nature.com/reprints.

Correspondence and requests for materials should be addressed to A.P.R. or S.F.

How to cite this article: Goldstein, E. A., Raman, A. P. & Fan, S. Sub-ambient non-evaporative fluid cooling with the sky. *Nat. Energy* **2,** 17143 (2017).

Publisher's note: Springer Nature remains neutral with regard to jurisdictional claims in published maps and institutional affiliations.

Competing interests

The authors have founded a company, SkyCool Systems, seeking to commercialize the results reported in this paper.

© 2017 Macmillan Publishers Limited, part of Springer Nature. All rights reserved.